LETTER

doi:10.1038/nature09607

c-Jun N-terminal phosphorylation antagonises recruitment of the Mbd3/NuRD repressor complex

Cristina Aguilera[1]*, Kentaro Nakagawa[1,2]*, Rocio Sancho[1], Atanu Chakraborty[1], Brian Hendrich[3] & Axel Behrens[1]

AP-1 (activator protein 1) activity is strongly induced in response to numerous signals, including growth factors, cytokines and extracellular stresses[1]. The proto-oncoprotein c-Jun belongs to the AP-1 group of transcription factors and it is a crucial regulator of intestinal progenitor proliferation and tumorigenesis[2–4]. An important mechanism of AP-1 stimulation is phosphorylation of c-Jun by the Jun amino-terminal kinases (JNKs)[1]. N-terminal phosphorylation of the c-Jun transactivation domain increases target gene transcription[5,6], but a molecular explanation was elusive. Here we show that unphosphorylated, but not N-terminally phosphorylated c-Jun, interacts with Mbd3 and thereby recruits the nucleosome remodelling and histone deacetylation (NuRD) repressor complex. Mbd3 depletion in colon cancer cells increased histone acetylation at AP-1-dependent promoters, which resulted in increased target gene expression. The intestinal stem cell marker *lgr5* was identified as a novel target gene controlled by c-Jun/Mbd3. Gut-specific conditional deletion of *mbd3* (*mbd3*$^{\Delta G/\Delta G}$ mice) stimulated c-Jun activity and increased progenitor cell proliferation. In response to inflammation, *mdb3* deficiency resulted in colonic hyperproliferation and *mbd3*$^{\Delta G/\Delta G}$ mice showed markedly increased susceptibility to colitis-induced tumorigenesis. Notably, concomitant inactivation of a single allele of *c-jun* reverted physiological and pathological hyperproliferation, as well as the increased tumorigenesis in *mbd3*$^{\Delta G/\Delta G}$ mice. Thus the transactivation domain of c-Jun recruits Mbd3/NuRD to AP-1 target genes to mediate gene repression, and this repression is relieved by JNK-mediated c-Jun N-terminal phosphorylation.

We described a yeast three-hybrid approach to identify proteins that interact with c-Jun depending on its phosphorylation status previously[7]. Mbd3 was cloned as an interactor that specifically bound to unphosphorylated c-Jun. Mbd3, together with Mbd1, 2 and 4, was originally characterized as a protein containing a region with high homology to the methyl-CpG-binding domain (MBD) of MeCP2. Mbd2 and Mbd3 assemble into mutually exclusive distinct NuRD complexes[8]. NuRD mediates gene repression through histone deacetylation via HDAC1 and 2, and chromatin remodelling ATPase activities through its CHD3 (Mi2α) and CHD4 (Mi2β) subunits[9–11]. Whereas Mbd2 recruits NuRD to methylated DNA, the MBD of Mbd3 fails to bind methylated DNA[12,13]. Thus, how Mbd3 interacts with chromatin to regulate transcription was not known.

Overexpressed c-Jun co-immunoprecipitated with Mbd3 but JNK activation by anisomycin (Ans) reduced the interaction of wild-type c-Jun and Mbd3. In contrast, a c-Jun4A mutant, in which the four N-terminal residues phosphorylated by JNK, serines 63 and 73, and threonines 91 and 93, are mutated into alanines, remained bound to Mbd3 despite high JNK activity (Fig. 1a). c-Jun4A also interacted more efficiently with CHD3 and MTA3, two major components of the NuRD complex (Supplementary Fig. 1a). Interaction of endogenous Mbd3 with c-Jun could not be detected when JNK activity was stimulated by ultraviolet light, but pharmacological JNK inhibition (JNKi), which resulted in a significant decrease in c-Jun N-terminal phosphorylation (Supplementary Fig. 2a), stimulated Mbd3 binding to c-Jun (Supplementary Fig. 1b). Moreover, recombinant glutathione-*S*-transferase

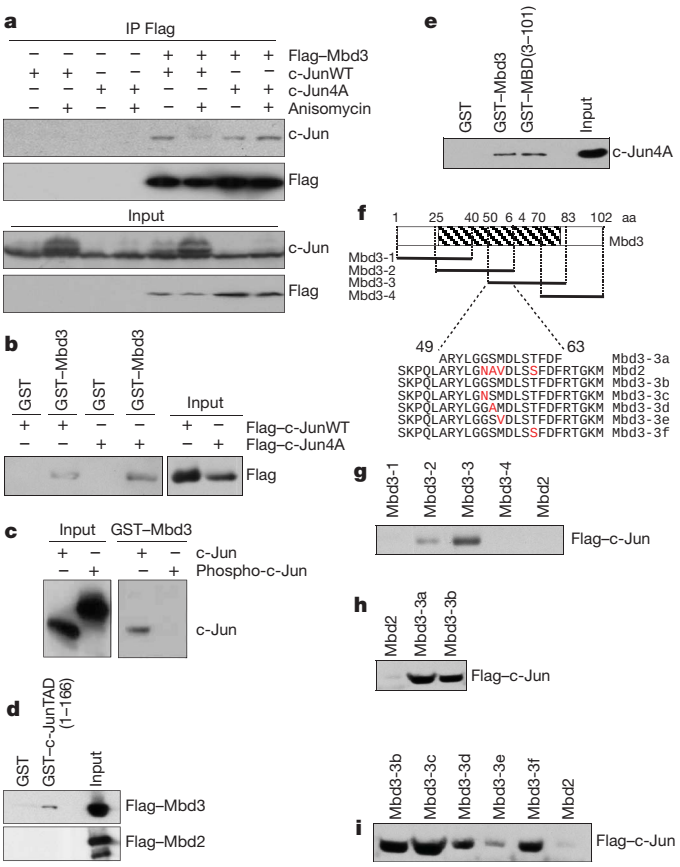

Figure 1 | Mbd3 interacts with unphosphorylated c-Jun through its MBD. **a**, HCT116 cells transfected with Myc–c-JunWT or Myc–c-Jun4A along with Flag–Mbd3 were treated with anisomycin for 1 h where indicated. Cell lysates were used to immunoprecipitate (IP) Flag–Mbd3. **b**, Pull-down experiment using GST–Mbd3 with HCT116 cell lysates transfected with c-JunWT or c-Jun4A. **c**, Pull-down experiment using GST–Mbd3 as a bait with recombinant c-Jun (c-Jun) or recombinant c-Jun that was phosphorylated *in vitro* by incubation with activated JNK1 protein (Phospho-c-Jun). **d**, Pull-down experiment using GST–JunTAD(1–166) with HCT116 cell lysates transfected with Flag–Mbd3 or Flag–Mbd2. **e**, Pull-down experiment using GST–Mbd3 or GST–MBD with HCT116 cell lysates transfected with Myc–c-Jun4A. **f**, Schematic overview of Mbd3 peptides covering the MBD, mutations are highlighted in red. **g–i**, Pull-down experiments using different biotinylated peptides shown in **f** with HEK293T cell lysates expressing Flag–c-Jun.

[1]Mammalian Genetics Laboratory, Cancer Research UK London Research Institute, Lincoln's Inn Fields Laboratories, 44 Lincoln's Inn Fields, London WC2A 3PX, UK. [2]Department of Medical Biochemistry, Graduate School of Medicine, Tokyo Medical and Dental University, 1-5-45 Yushima, Bunkyo-ku, Tokyo 113-8519, Japan. [3]Wellcome Trust Centre for Stem Cell Research, Medical Research Council Centre for Stem Cell Biology and Regenerative Medicine, Department of Biochemistry, University of Cambridge, Tennis Court Road, Cambridge CB2 1QR, UK.
*These authors contributed equally to this work.

(GST)–Mbd3 interacted more efficiently with c-Jun4A than with wild-type c-Jun (Fig. 1b). Bacterially produced GST–Mbd3 bound to recombinant c-Jun, but this interaction was reduced by *in vitro* phosphorylation of recombinant c-Jun by activated JNK1 (Fig. 1c). GST pull-down assays showed that the transactivation domain (TAD, amino acid residues 1–166) of c-Jun was sufficient to bind Mbd3, but did not interact with the closely related Mbd2 protein (Fig. 1d). The delta (δ) domain of c-Jun (residues 31–60), which is required for JNK binding, was dispensable for Mbd3 interaction, and further mapping identified the region between residues 60 and 120, which encompasses the JNK phosphoacceptor residues, as the Mbd3 binding site of c-Jun (Supplementary Fig. 1c–e). Thus, Mbd3 binds directly and preferentially to the unphosphorylated TAD of c-Jun, and this interaction is disrupted by phosphorylation.

To determine the domain of Mbd3 involved in binding to c-Jun, serial deletion mutants of Mbd3 were generated (Supplementary Fig. 3a). The deletion of residues 40 to 80 of Mbd3, which encode part of the MBD, reduced Mbd3 binding to c-Jun (Supplementary Fig. 3b). Recombinant Mbd3 MBD (GST–MBD(3–101)) bound to c-Jun as efficiently as full-length Mbd3 (GST–Mbd3) (Fig. 1e). Using overlapping biotinylated peptides covering the Mbd3 MBD we identified the region from residue 49 to residue 63 as crucial for Mbd3 binding to c-Jun (Fig. 1f, g and Supplementary Fig. 4a). A 15-residue peptide covering this region was sufficient to mediate c-Jun interaction (Fig. 1h). This region differs only in four residues to the same region in Mbd2 and a peptide with the corresponding Mbd2 sequence did not bind c-Jun (Fig. 1h). Single amino acid changes revealed a large contribution of methionine 56 and to a lesser extent serine 55 of Mbd3 in c-Jun binding (Fig. 1i and Supplementary Fig. 4b). Thus, the MBD of Mbd3 is necessary and sufficient for c-Jun binding, indicating that the MBD of Mbd3 has evolved from a methyl-CpG-binding domain into a protein–protein interaction module.

To investigate the role of Mbd3 in regulating c-Jun function, we knocked-down *mbd3* with a small hairpin RNA (shRNA) construct (Supplementary Fig. 2b) and transfected it along with a luciferase reporter construct driven by an artificial promoter consisting of multimerized AP-1 site (AP-1 luciferase) to assess c-Jun transcriptional activity. The knock-down of *mbd3* induced an increase in reporter gene activity (Fig. 2a). Similar results were obtained using the urokinase-type plasminogen activator promoter (uPA-luciferase) (Supplementary Fig. 5a), a well known AP-1 target gene[14].

c-jun transcription is induced very quickly in response to JNK activation and c-Jun autoregulates its own promoter via two proximal AP-1 binding sites[15]. Chemical JNKi (Fig. 2b) or expression of *jnk1/2*-specific (also known as *MAPK8/9*) shRNAs, which resulted in substantial depletion of JNK protein (Supplementary Fig. 2c), decreased endogenous *c-jun* mRNA levels but *c-jun* transcriptional repression by JNK inhibition was impaired in the absence of Mbd3 (Fig. 2b and Supplementary Fig. 5b). Moreover, overexpression of Flag–Mbd3 decreased transcriptional activation of *c-jun* and, to a lesser extent, *cd44*, which is also regulated by c-Jun[4] (Supplementary Fig. 5d, e). Thus, depletion of Mbd3 results in derepression of AP-1 activity.

HCT116 colon cancer cells have constitutively high levels of activated JNK and phosphorylated c-Jun (Supplementary Fig. 2a) and chromatin immunoprecipitation (ChIP) for Mbd3 revealed minimal binding to a region covering the AP-1 sites of the *c-jun* promoter. However, JNKi and *jnk1/2* depletion resulted in a rapid and efficient recruitment of Mbd3 to the *c-jun* promoter (Fig. 2c and Supplementary Fig. 6a) and the *cd44* promoter (Supplementary Fig. 6b, c). Thus, the JNK signalling pathway regulates Mbd3 recruitment to c-Jun-dependent promoters.

ChIP analysis demonstrated that HDAC1 was also recruited to the *c-jun* promoter after JNKi and knock-down of Mbd3 prevented this recruitment (Fig. 2d). Unphosphorylatable c-Jun4A protein recruited Mbd3 more efficiently to the *c-jun* promoter compared to wild-type c-Jun (c-JunWT) (Supplementary Fig. 6d). c-Jun4A also recruited more HDAC1 to the *c-jun* promoter, and this recruitment was prevented when Mbd3 was silenced (Fig. 2e).

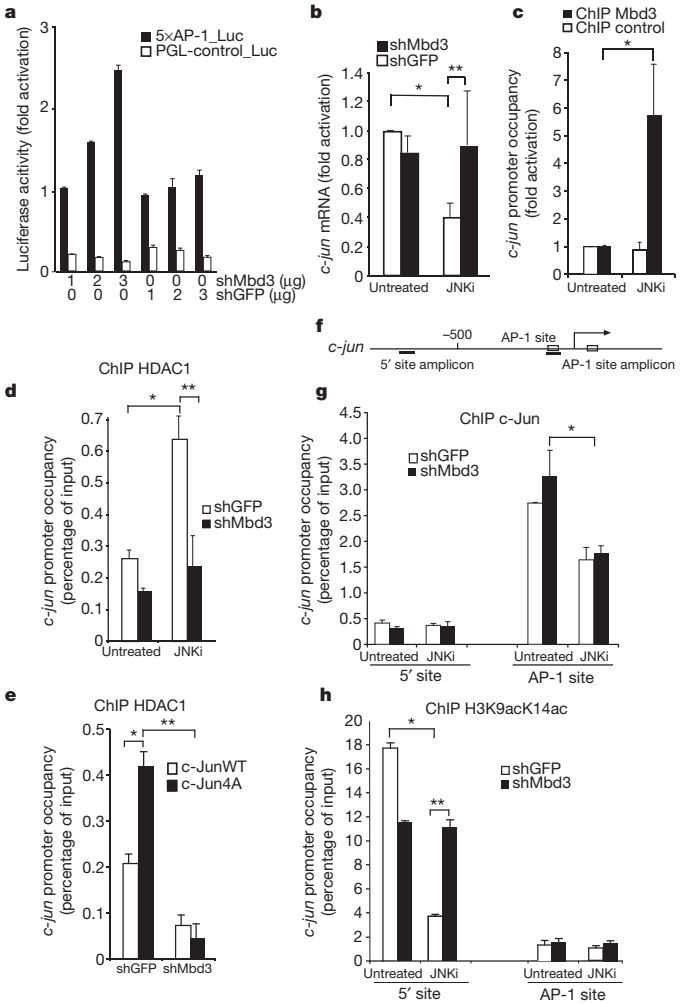

Figure 2 | Mbd3 represses *c-jun* transcription. **a**, Cells were transfected with a pSUPER vector expressing a shRNA specific for Mbd3 (shMbd3) or for GFP (shGFP). Activity of a 5×AP-1 luciferase reporter construct (5×AP-1_luc) or empty vector (PGL-control_Luc) relative to a thymidine kinase *Renilla* luciferase transfection control (tk-renilla) is shown ($n = 3$). **b**, mRNA levels of *c-jun* in the presence or absence of shMBD3 with JNKi or mock treatment ($n = 5$; $^*P = 0.001$; $^{**}P = 0.03$). **c**, ChIP for the AP-1 site in the *c-jun* promoter using Mbd3-specific or control antibody with or without JNKi ($n = 9$; $^*P = 0.043$). **d**, HDAC1 ChIP for the AP-1 site in the *c-jun* promoter on cells expressing a shRNA specific for Mbd3 or for GFP ($^*P = 0.004$; $^{**}P = 0.0003$). **e**, HDAC1 ChIP for the *c-jun* AP-1 sites on cells expressing wild-type c-Jun (c-JunWT) or c-Jun4A ($^*P = 0.02$; $^{**}P = 0.01$). **f**, Schematic overview of the *c-jun* promoter. Underlined regions show the amplification region of each primer pair used. **g**, c-Jun ChIP for the 5′ and AP-1 sites of the *c-jun* locus on cells expressing a shRNA specific for Mbd3 or for GFP ($^*P = 0.02$). **h**, ChIP for acetylated histone 3 K9, 14 (H3K9acK14ac) as in **g** ($^*P = 0.0002$; $^{**}P = 0.006$). In all experiments error bars show s.e.m. and Student's *t*-test was used for statistical analysis. HCT116 cells were used throughout. JNKi treatment was for 2 h in **b**, and for 30 min in **c**, **d**, **g** and **h**.

Histone acetylation has an important role in *c-jun* transcriptional regulation[16]. It has been shown previously that the regulation of histone acetylation at the *c-jun* promoter is complex. Increased histone acetylation in response to JNK activation was observed in a more distal region of the promoter (5′ site), whereas the region around the AP-1 sites remained unchanged[16] (Fig. 2f). In agreement with previous observations, we detected substantial histone H3 acetylation in the 5′ area of the promoter by ChIP, but no significant H3 acetylation around the AP-1 sites where c-Jun is localized (Fig. 2g, h). As expected, JNK inhibition induced a marked decrease in histone H3 acetylation,

but the regulation of H3 acetylation at the *c-jun* promoter was disrupted by Mbd3 depletion. H3 acetylation was slightly reduced in untreated cells, but in response to JNK inhibition no decrease in H3 acetylation was observed (Fig. 2h). Thus, Mbd3 contributes to the epigenetic regulation of the *c-jun* promoter by JNK signalling.

c-Jun has an important function in regulating intestinal epithelial homeostasis and intestinal cancer[3,4]. Quantitative real-time polymerase chain reaction (qRT-PCR) analysis revealed an enrichment of *mbd3* mRNA in intestinal crypts (Supplementary Fig. 7a), and analysis of a knock-in mouse that expresses the reporter protein β-galactosidase under the control of the endogenous *mbd3* promoter (Supplementary Fig. 8a)[17] confirmed high *mdb3* expression in the crypt (Supplementary Fig. 7b). To address a potential role of Mbd3 in controlling c-Jun function in the intestine, we generated a mouse line in which exon 1 of Mbd3 was flanked with two *loxP* sites (Supplementary Fig. 8a). Exon 1 of Mbd3 encodes the N-terminal portion of the MBD and after Cre-mediated recombination *mbd3a* and *mbd3b*, the two transcripts generated from the *mbd3* locus, are not produced (Supplementary Fig. 8b, c). We crossed the Mbd3 floxed mouse line with a Villin-Cre line[18] to specifically inactivate *mbd3* in the gut ($mbd3^{\Delta G/\Delta G}$). Deletion of the floxed *mbd3* allele was efficient (Supplementary Fig. 8d) and mRNA was isolated from crypts to investigate AP-1-dependent gene expression. Transcription of *c-jun* was increased in intestinal crypts lacking Mbd3, as was the transcription of several c-Jun target genes including *cd44* and *cyclind1* (also known as *Ccnd1*)(Fig. 3a). In addition, the expression of the stem cell marker *lgr5* was also increased in $mbd3^{\Delta G/\Delta G}$ intestine (Fig. 3a) whereas *bmi1* remained unchanged. *lgr5* marks crypt base columnar (CBC) cells, which function as intestinal stem cells[19]. The increase in *lgr5* mRNA was not due to an increase of CBC cells as their number was normal in the absence of Mbd3 (Fig. 3b). c-Jun is highly expressed in CBC cells[3,20], and *lgr5* expression is reduced in crypts lacking c-Jun[3]. We thus analysed whether *lgr5* might be directly regulated by c-Jun/Mbd3. *In silico* analysis revealed the presence of a consensus AP-1 site in intron 1 of the *lgr5* gene (Fig. 3c) and ChIP analysis

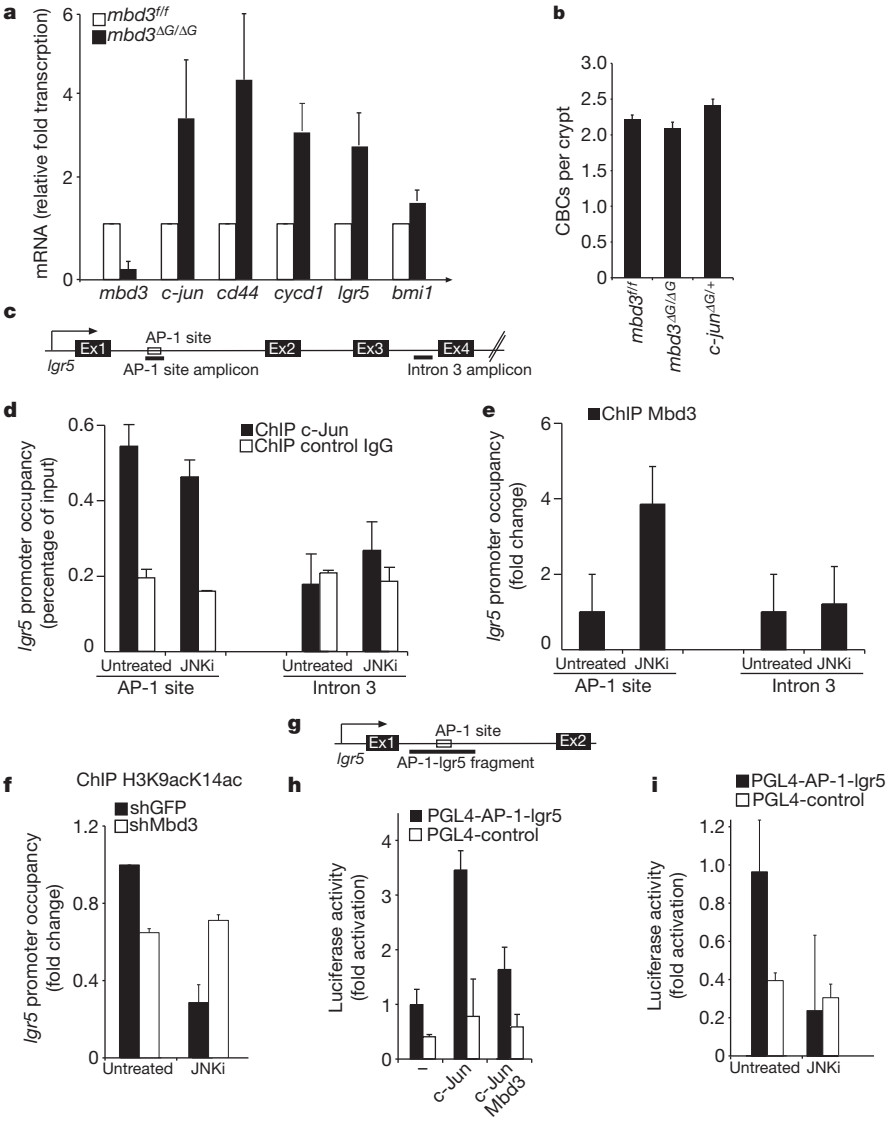

Figure 3 | *lgr5* is regulated by c-Jun-Mbd3/NuRD. **a**, qRT-PCR analysis of indicated genes on mRNA isolated from intestines of $mbd3^{f/f}$ and $mbd3^{\Delta G/\Delta G}$ mice ($n = 4$). Data were normalized to β-actin. **b**, Quantification of crypt base columnar cells (CBC) in $mbd3^{f/f}$ ($n = 4$), $mbd3^{\Delta G/\Delta G}$ ($n = 3$) and $mbd3^{\Delta G/\Delta G}$-$jun^{\Delta G/+}$ ($n = 3$) mice. **c**, Schematic overview of the *lgr5* locus. Underlined regions show the amplification region of each primer pair used. **d**, ChIP for the *lgr5* AP-1 and intron 3 sites using c-Jun-specific or control antibody with or without JNKi. **e**, Mbd3 ChIP for the AP-1 and intron 3 sites in the *lgr5* locus. **f**, Mbd3 ChIP for the *lgr5* AP-1 site with or without JNKi. **g**, Schematic overview of the fragment used for AP-1-lgr5 luciferase construct. **h**, **i**, Activity of an AP-1-lgr5 luciferase construct (PGL4-AP-1-lgr5) or empty vector (PGL4-control_Luc) relative to a tk-renilla luciferase transfection control in cells expressing c-Jun and Mbd3 (**h**) or with or without JNKi treatment (**i**). In all experiments (**c**–**f**, **h** and **i**) error bars show s.e.m. HCT116 cells were used and $n = 3$. JNKi treatment was for 30 min in **d**–**f** and for 5 h in **i**.

showed binding of c-Jun to this putative AP-1 site, but not to a region in intron 3 of the *lgr5* gene, used as a negative control (Fig. 3d). Mbd3 was also recruited to the same site in intron 1 of the *lgr5* gene, and JNKi increased Mbd3 recruitment (Fig. 3e). In addition, JNKi augmented CHD3 binding to the *lgr5* and *c-jun* AP-1 sites to a similar extent (Supplementary Fig. 6e, f). JNK inhibition reduced acetylation of the *lgr5* AP-1 site but the Mbd3 depletion impaired JNKi-induced deacetylation (Fig. 3f). When inserted into a luciferase reporter construct, the *lgr5* fragment containing the AP-1 site (pGL4-Ap-1-lgr5) (Fig. 3g) was activated by c-Jun overexpression whereas coexpression with Mbd3 resulted in repression (Fig. 3h). JNKi reduced pGL4-Ap-1-lgr5 reporter activity to background levels (Fig. 3i). These data suggest that Mbd3/c-Jun regulates *lgr5* transcription.

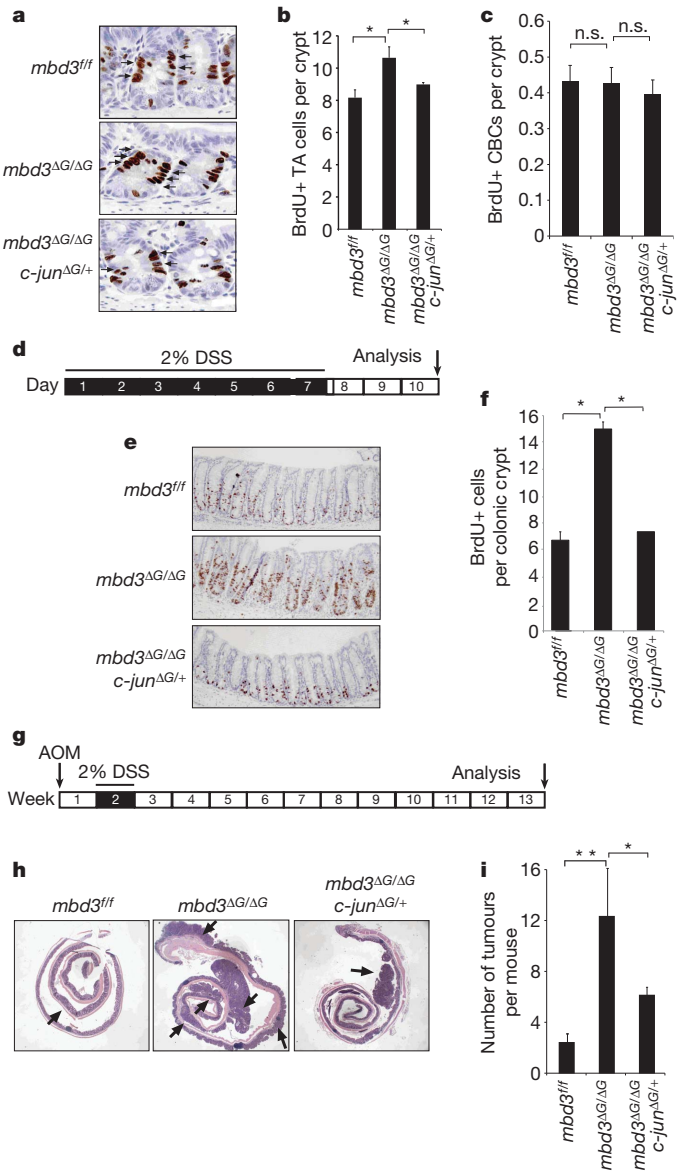

Figure 4 | Mbd3 antagonises c-Jun/AP-1 function *in vivo*.
a, Immunohistochemistry for BrdU+ cells on representative crypts of the indicated genotypes. Black arrows point to BrdU+ proliferative progenitors. **b**, Quantification of BrdU-positive (BrdU+) transit amplifying (TA) cells in $mbd3^{f/f}$ ($n = 6$), $mbd3^{\Delta G/\Delta G}$ ($n = 5$) and $mbd3^{\Delta G/\Delta G}c\text{-}jun^{\Delta G/+}$ ($n = 4$) in intestinal crypts (error bars show s.e.m.; $^*P = 0.001$; Student's *t*-test). **c**, Quantification of BrdU+ CBCs in $mbd3^{f/f}$ ($n = 4$), $mbd3^{\Delta G/\Delta G}$ ($n = 3$) and $mbd3^{\Delta G/\Delta G}c\text{-}jun^{\Delta G/+}$ ($n = 3$) intestinal crypts. n.s., not significant. **d**, Schematic representation of the experimental design for DSS-induced intestinal regeneration. **e**, Immunohistochemistry for BrdU+ cells on representative colonic crypts of mice with the indicated genotypes. **f**, Quantification of $BrdU^+$ cells in $mbd3^{f/f}$ ($n = 10$), $mbd3^{\Delta G/\Delta G}$ ($n = 6$) and $mbd3^{\Delta G/\Delta G}c\text{-}jun^{\Delta G/+}$ ($n = 2$) mice colonic crypts; $^*P = 0.00012$. **g**, Schematic representation of the experimental design for colitis-induced tumorigenesis. **h**, Haematoxylin and eosin staining on representative colons of mice with the indicated genotypes. **i**, Quantification of number of AOM/DSS-induced tumours in $mbd3^{f/f}$ ($n = 5$), $mbd3^{\Delta G/\Delta G}$ ($n = 4$) and $mbd3^{\Delta G/\Delta G}c\text{-}jun^{\Delta G/+}$ ($n = 2$) mice ($^{**}P = 0.01$, $^*P = 0.016$). In all experiments error bars show s.e.m. and Student's *t*-test was used for statistical analysis.

The only described biological function of Mbd3 is in controlling proliferation and differentiation of embryonic stem cells[21,22], so we investigated whether intestinal cell lineage specification was impaired in the gut of $mbd3^{\Delta G/\Delta G}$ mice. Immunohistochemical stainings for Alcian blue/periodic acid Schiff (AB/PAS) (which detects goblet cells), chromogranin (for enteroendocrine cells) or lysozyme (for Paneth cells) failed to detect a defect in cell fate specification in the intestine of $mbd3^{\Delta G/\Delta G}$ mice (Supplementary Fig. 9a–c). Interestingly, $mbd3^{\Delta G/\Delta G}$ mice showed a significant increase in bromodeoxyuridine (BrdU)-positive transient amplifying cells in the crypts compared to controls (Fig. 4a, b), but we did not detect any increase in CBC cell proliferation (Fig. 4c). To test whether increased c-Jun activity was responsible for the augmented intestinal progenitor proliferation in $mbd3^{\Delta G/\Delta G}$ mice, one *c-jun* allele was deleted in a $mbd3^{\Delta G/\Delta G}$ background, generating $mbd3^{\Delta G/\Delta G}$; $c\text{-}jun^{\Delta G/+}$ mice. The hyperproliferation phenotype in the absence of Mbd3 was rescued in $mbd3^{\Delta G/\Delta G}$; $c\text{-}jun^{\Delta G/+}$ mice (Fig. 4a, b). We next investigated the impact of *mbd3* inactivation under pathological conditions. Intestinal colitis and regeneration was induced by dextran sodium sulphate (DSS) administration (Fig. 4d). $mbd3^{\Delta G/\Delta G}$ mice showed a large increase in proliferating cells in the colon after DSS treatment compared to control animals. The hyperproliferation phenotype was completely reversed by deletion of a single *c-jun* allele (Fig. 4e, f). Moreover, to investigate a potential role of Mbd3 in intestinal tumorigenesis, we applied the azoxymethane (AOM)/DSS protocol to trigger colitis-induced tumorigenesis (Fig. 4g)[3]. Mbd3 deletion resulted in a striking increase in tumour number (Fig. 4h, i) as well as an increase in tumour size (Supplementary Fig. 9d) that was significantly rescued by concomitant deletion of one *c-jun* allele (Fig. 4h, i and Supplementary Fig. 9d). Thus, in the intestine Mbd3 controls cellular proliferation under physiological and pathological conditions by antagonising c-Jun activity.

The direct recruitment of the NuRD complex by Mbd3 interaction with unphosphorylated c-Jun suggests that in the absence of JNK pathway activation, c-Jun actively represses AP-1 target gene expression, providing a molecular explanation for previous observations that c-Jun phosphorylation mediates dissociation of an inhibitory complex associated with histone deacetylation[23,24]. The phosphorylation-dependent interaction of Mbd3/c-Jun is in agreement with a three-step mechanism of c-Jun activation by JNK. Upon JNK activation, NuRD dissociates from c-Jun, resulting in derepression of target gene transcription. Subsequently, a coactivator protein would bind to the c-Jun TAD and further augment gene expression. It is worth noting that to explain stimulation of c-Jun activity by N-terminal phosphorylation, coactivator binding may, but is not required to be phosphorylation-dependent[4,25]. Lastly, upon termination of the JNK signal, Mbd3/NuRD would re-bind to unphosphorylated c-Jun resulting in cessation of target gene expression. Thus, the TAD of c-Jun functions as a repressor domain that is negatively regulated by phosphorylation.

METHODS SUMMARY

Cell culture. HCT116 and HEK293T cells were grown in DMEM and 10% FBS.
IP, pull-down and western blot analysis. Cells were lysed in the appropriate buffer for immunoprecipitation, GST pull-down or peptide pull-down assays. Immunoblots were carried out as previously described[4].
Reporter gene assay. Firefly and *Renilla* luciferase reporter assays were performed and measured using the Dual-Luciferase Reporter Assay System (Promega).
Chromatin immunoprecipitation (ChIP). ChIP analysis was performed as described previously[26]. qRT-PCR was accomplished with SYBR Green incorporation.

Mouse lines. Mbd3$^{\Delta G/\Delta G}$ mice resulted from crossing Mbd3 floxed line[21] with villin cre line[18].

AOM/DSS model of colon carcinoma and DSS model of colon inflammation. The AOM/DSS model[27] and the DSS protocol used[28] have been previously described. For tissue collection, mice were sacrificed and the intestines were frozen in liquid nitrogen. For qRT–PCR analysis, total mRNA was isolated from dissected intestines, or from villus and crypt fractions obtained as described before[19].

Immunohistochemical staining. For haematoxylin & eosin staining and immunohistochemistry, the intestines were fixed overnight in 10% neutral buffered formalin, transferred into 70% ethanol, rolled, processed and embedded into paraffin. Sections were cut at 4 μm.

Full Methods and any associated references are available in the online version of the paper at www.nature.com/nature.

Received 1 September; accepted 25 October 2010.
Published online 2 January 2011.

1. Davis, R. J. Signal transduction by the JNK group of MAP kinases. *Cell* **103,** 239–252 (2000).
2. Eferl, R. & Wagner, E. F. AP-1: a double-edged sword in tumorigenesis. *Nature Rev. Cancer* **3,** 859–868 (2003).
3. Sancho, R. *et al.* JNK signalling modulates intestinal homeostasis and tumourigenesis in mice. *EMBO J.* **28,** 1843–1854 (2009).
4. Nateri, A. S., Spencer-Dene, B. & Behrens, A. Interaction of phosphorylated c-Jun with TCF4 regulates intestinal cancer development. *Nature* **437,** 281–285 (2005).
5. Pulverer, B. J., Kyriakis, J. M., Avruch, J., Nikolakaki, E. & Woodgett, J. R. Phosphorylation of c-jun mediated by MAP kinases. *Nature* **353,** 670–674 (1991).
6. Behrens, A., Sibilia, M. & Wagner, E. F. Amino-terminal phosphorylation of c-Jun regulates stress-induced apoptosis and cellular proliferation. *Nature Genet.* **21,** 326–329 (1999).
7. Nateri, A. S., Riera-Sans, L., Da Costa, C. & Behrens, A. The ubiquitin ligase SCFFbw7 antagonizes apoptotic JNK signaling. *Science* **303,** 1374–1378 (2004).
8. Le Guezennec, X. *et al.* MBD2/NuRD and MBD3/NuRD, two distinct complexes with different biochemical and functional properties. *Mol. Cell. Biol.* **26,** 843–851 (2006).
9. Denslow, S. A. & Wade, P. A. The human Mi-2/NuRD complex and gene regulation. *Oncogene* **26,** 5433–5438 (2007).
10. Ahringer, J. NuRD and SIN3 histone deacetylase complexes in development. *Trends Genet.* **16,** 351–356 (2000).
11. Bowen, N. J., Fujita, N., Kajita, M. & Wade, P. A. Mi-2/NuRD: multiple complexes for many purposes. *Biochim. Biophys. Acta* **1677,** 52–57 (2004).
12. Saito, M. & Ishikawa, F. The mCpG-binding domain of human MBD3 does not bind to mCpG but interacts with NuRD/Mi2 components HDAC1 and MTA2. *J. Biol. Chem.* **277,** 35434–35439 (2002).
13. Hendrich, B. & Tweedie, S. The methyl-CpG binding domain and the evolving role of DNA methylation in animals. *Trends Genet.* **19,** 269–277 (2003).
14. D'Orazio, D. *et al.* Cooperation of two PEA3/AP1 sites in uPA gene induction by TPA and FGF-2. *Gene* **201,** 179–187 (1997).
15. Angel, P., Hattori, K., Smeal, T. & Karin, M. The *jun* proto-oncogene is positively autoregulated by its product, Jun/AP-1. *Cell* **55,** 875–885 (1988).
16. Clayton, A. L., Rose, S., Barratt, M. J. & Mahadevan, L. C. Phosphoacetylation of histone H3 on c-*fos*- and c-*jun*-associated nucleosomes upon gene activation. *EMBO J.* **19,** 3714–3726 (2000).
17. Hendrich, B., Guy, J., Ramsahoye, B., Wilson, V. A. & Bird, A. Closely related proteins MBD2 and MBD3 play distinctive but interacting roles in mouse development. *Genes Dev.* **15,** 710–723 (2001).
18. El Marjou, F. *et al.* Tissue-specific and inducible Cre-mediated recombination in the gut epithelium. *Genesis* **39,** 186–193 (2004).
19. Barker, N. *et al.* Identification of stem cells in small intestine and colon by marker gene *Lgr5*. *Nature* **449,** 1003–1007 (2007).
20. van der Flier, L. G. *et al.* Transcription factor achaete scute-like 2 controls intestinal stem cell fate. *Cell* **136,** 903–912 (2009).
21. Kaji, K. *et al.* The NuRD component Mbd3 is required for pluripotency of embryonic stem cells. *Nature Cell Biol.* **8,** 285–292 (2006).
22. Kaji, K., Nichols, J. & Hendrich, B. Mbd3, a component of the NuRD co-repressor complex, is required for development of pluripotent cells. *Development* **134,** 1123–1132 (2007).
23. Baichwal, V. R., Park, A. & Tjian, R. The cell-type-specific activator region of c-Jun juxtaposes constitutive and negatively regulated domains. *Genes Dev.* **6,** 1493–1502 (1992).
24. Weiss, C. *et al.* JNK phosphorylation relieves HDAC3-dependent suppression of the transcriptional activity of c-Jun. *EMBO J.* **22,** 3686–3695 (2003).
25. Arias, J. *et al.* Activation of cAMP and mitogen responsive genes relies on a common nuclear factor. *Nature* **370,** 226–229 (1994).
26. Nelson, J. D., Denisenko, O. & Bomsztyk, K. Protocol for the fast chromatin immunoprecipitation (ChIP) method. *Nature Protocols* **1,** 179–185 (2006).
27. Neufert, C., Becker, C. & Neurath, M. F. An inducible mouse model of colon carcinogenesis for the analysis of sporadic and inflammation-driven tumor progression. *Nature Protocols* **2,** 1998–2004 (2007).
28. Floer, M. *et al.* Enoxaparin improves the course of dextran sodium sulfate-induced colitis in syndecan-1-deficient mice. *Am. J. Pathol.* **176,** 146–157 (2010).

Supplementary Information is linked to the online version of the paper at www.nature.com/nature.

Acknowledgements We are grateful to the LRI Animal Unit, Equipment Park, FACS, Peptide synthesis and the Experimental Histopathology unit for technical help and O. S. Gabrielsen for reagents. We thank C. Hill and H. Van Dam for critical reading of the manuscript. C.A. and R.S. were funded by Marie Curie Intraeuropean Fellowships (PIEF-GA-2008-220566 and MEIF-CT-2006-041119). The London Research Institute is funded by Cancer Research UK.

Author Contributions C.A. designed and performed most of the experiments, analysed data, and co-wrote the paper. K.N. identified Mbd3 as binding specifically to unphosphorylated c-Jun using the yeast three-hybrid screen, generated reagents and provided Fig. 1a, c and Supplementary Fig. 3. R.S. helped with all *in vivo* experiments and provided Fig. 3a and Supplementary Fig. 7a. A.C. provided Fig. 1f–i. B.H. generated the *mbd3* floxed mouse line. A.B. supervised all aspects of this work and wrote the paper.

Author Information Reprints and permissions information is available at www.nature.com/reprints. The authors declare no competing financial interests. Readers are welcome to comment on the online version of this article at www.nature.com/nature. Correspondence and requests for materials should be addressed to axel.behrens@cancer.org.uk

METHODS

Cell culture and transfection. HCT116 and HEK293T cells were cultured in Dulbeccos's modified Eagle medium (DMEM) and 10% FBS. Cells were plated at subconfluence and transfected with lipofectamine reagent (Invitrogen). HCT116 cells were treated when indicated with 50 μM JNKi (SP600125, Calbiochem) or 25 ng ml^{-1} anisomycin (Sigma).

Immunoprecipitation. Cells were lysed for 30 min at 4 °C in 500 μl of immunoprecipitation buffer containing 0.5% Triton X-100, 1 mM EDTA, 100 μM Na-orthovanadate, 0.25 mM PMSF (phenylmethylsulphonyl fluoride), and protease inhibitor mixture (Sigma) in PBS. After centrifugation, supernatants were incubated for 3 h at 4 °C with 1 μg of the anti-Flag (Sigma) antibody coupled to protein A-Sepharose beads.

GST pull-down. GST fusion proteins were purified from the *Escherichia coli* BL-21 strain in a buffer containing 20 mM Tris-HCl, pH 7.4, 1 M NaCl, 0.2 mM EDTA, 1 mM dithiothreitol (DTT), 1 mg ml^{-1} lysozyme, 1 mM PMSF, and protease inhibitor complex (Sigma) and bound to glutathione-Sepharose (Amersham Biosciences). GST fusion proteins were purified and incubated with 400 μg of cell lysates for 2 h at 4 °C in RIPA buffer and extensively washed. Pulled down proteins were analysed by western blot.

Peptide pull-down. Biotinylated peptide (1 mg) was incubated with Dynabeads M280 streptavidin in buffer A (5 mM Tris-Cl pH 7.5, 0.5 mM EDTA, 1 M NaCl) at 4 °C overnight. Peptide bound beads were washed and resuspended in lysis buffer (20 mM Tris-HCl pH 8.0, 150 mM NaCl, 0.2% NP 40, 1 mM DTT). 293T cells overexpressing c-Jun were lysed in lysis buffer and then incubated with different Dynabead-bound peptides for 2 h at 4 °C. The beads were washed three times with lysis buffer containing 400 mM NaCl. Pulled-down proteins were analysed by western blot.

Western blot analysis. HCT116 cells lysates were homogenized in RIPA lysis buffer supplemented with protease inhibitor (Sigma). Immunoblots were carried out as described previously[4]. The gels were transferred to nitrocellulose membranes, and the membranes were immunoblotted with various antibodies as indicated: anti-c-Jun (H79, Santa Cruz sc1694 and BD Transduction Laboratories 610326), anti-Myc (9E10 clone), anti-Flag–HRP (horseradish peroxidase-conjugated; Sigma), anti-c-Jun-ser63 and anti-β-Actin (Sigma), anti-Mbd3 (c-18, Santa Cruz sc-9402), anti-JNK1/2 (NEB cell signalling 9252), anti-CHD3 (BD Transduction Laboratories 611847) and anti-MTA3 (Santa Cruz sc- 48799). HCT116 cells were treated where indicated with ultraviolet at 40 J cm^{-2}.

Reporter gene assay. HCT116 cells were transfected with the indicated plasmids with lipofectamine reagent (Invitrogen). Transient transfections of the indicated plasmids and controls of firefly and *Renilla* luciferase reporters were performed and measured using the Dual-Luciferase Reporter Assay System (Promega), 36 h post-transfection. Data are expressed as fold induction after being normalized using tk-renilla luciferase (mean ± s.e.m.; $n = 3$).

Chromatin immunoprecipitation (ChIP). ChIP analysis was performed as described previously[26]. Cells were treated as indicated before collection, with 50 μM JNKi (SP600125, Calbiochem), 25 ng ml^{-1} anisomycin (Sigma) or transfected with the indicated plasmids with lipofectamine reagent (Invitrogen). Immunoprecipitations were carried out with the indicated antibodies, anti-Mbd3 (c-18) (Santa Cruz sc9402), anti-HDAC1 (H51) (Santa Cruz sc7872), anti-c-Jun (H79) (Santa Cruz sc1694) or anti-acetyl K9, K14 histone 3 (Upstate 06-599) and collected by agarose beads (Santa-Cruz). The oligonucleotide sequences used to amplify the DNA fragments by qRT-PCR are AP1 c-Jun F, 5′-GCGACGCGAGCCAATG-3′; AP1 c-Jun R, 5′-AGCCCGAGCTCAACAC TTATCT-3′; 5′ c-Jun F, 5′-TTATACTCCTCCTCCCCCAGCTA-3′; 5′ c-Jun R, 5′-CCTCCAGCCTCCTGAAACATC-3′; lgr5-AP-1 F, 5′-TGGGAATCA GTGCGGTTCA-3′; lgr5-AP-1 R, 5′-CAGGGAAATGGGCAAACAAG-3′; lgr5-intron3 F, 5′-TCTGCCTCAGGCTTACATGGA-3′; lgr5-intron3 R, 5′-CA CAAGAATTCTGCAGCACATTT-3′; F-CD44 AP-1, 5′-AGTGCAGTGGCACG ATCTTG-3′; R-CD44 AP-1, 5′-CGGGAGAATCGCTTGAACAC-3′.

Quantitative real-time PCR was performed with SYBR Green incorporation (Platinum Quantitative PCR SuperMix-UDG w/ROX, Invitrogen) using an ABI7900HT (Applied Bioscience) and the data were analysed using the SDS 2.3 software.

RNA extraction and qRT-PCR analysis. Total mRNA was isolated using RNeasy Mini-kit according to the manufacturer's instructions (Qiagen). cDNA was synthesized using Invitrogen Superscript reagents according to the manufacturer's instructions. The oligonucleotide sequences used to amplify the DNA fragments by qRT-PCR are F-h-c-Jun, 5′-TCGACATGGAGTCCCAGGA-3′; R-h-c-Jun, 5′-GGCGATTCTCTCCAGCTTCC-3′; F-h-actin, 5′-GGATGCAGAAGGAG ATCACTG-3′; R-h-actin, 5′-CGATCCACACGGAGTACTTG-3′; F-hCD44, 5′-CTCCTGGCACTGGCTCTGA-3′; R-hCD44, 5′-CTGCCCACACCTTCT CCTACTATT-3′; F-mMbd3, 5′-CACCGCGCTGCCTGTAC-3′; R-mMbd3, 5′-TGGTCACCGGTTGCTTGA-3′; F-mc-Jun, 5′-TGAAAGCTGTGTCCCC TGTC-3′; R-mc-Jun, 5′-ATCACAGCACATGCCACTTC-3′; F-mβ-actin, 5′-ATGCTCCCCGGGCTGTAT-3′; R-mβ-actin, 5′-CATAGGAGTCCTTCTG ACCCATTC-3′; F-mCD44, 5′-CTCCTGGCACTGGCTCTGA-3′; R-mCD44, 5′-CTGCCCACACCTTCTCCTACTATT-3′; F-mCCDN1, 5′-GTGCGTGCA GAAGGAGATTGT-3′; R-mCCDN1, 5′-CTCACAGACCTCCAGCATCCA-3′; F-mLgr5, 5′-CGGAGGAAGCGCTACAGAAT-3′; R-mLgr5, 5′-CTGGGT GGCACGTAGCTGAT-3′; F-mBmiI, 5′-GGGCTTTTCAAAAATGAGATGAA-3′; R-mBmiI, 5′-GAGCCATTGGCAGCATCAG-3′.

Quantitative real-time PCR was accomplished with SYBR Green incorporation (Platinum Quantitative PCR SuperMix-UDG w/ROX, Invitrogen) using an ABI7900HT (Applied Bioscience), and the data were analysed using the SDS 2.3 software. Results were normalized to those obtained with β-actin.

RNAi constructs. siRNA sequences directed towards the coding region of the indicated genes were designed using the Dharmacon siDESIGN centre. Annealed hairpin oligonucleotides were cloned into pSuper (OligoEngine).

shGFP, sense strand 5′-GAACGGCATCAAGGTGAAC-3′; shJNK1/2, sense strand 5′-AAAGAATGTCCTACCTTCTT-3′; shMbd3-a, sense strand 5′-AGA CGGCGTCCATCTTCAA-3′; shMbd3-b, sense strand 5′-TATGGCTCAAC ACCACGCA-3′; shMbd3-c, sense strand 5′-GGACATCAGGAAGCAGGAA-3′.

Mouse lines. Embryonic stem cells in which one *mbd3* allele is deleted and the other contains *loxP* sites flanking exon 1 have been described[21]. Upon transfection with Cre recombinase, the resulting *mbd3 Ex1*$^{\Delta/-}$ embryonic stem cells lack Mbd3a and Mbd3b. *mbd3*$^{Flox/-}$ embryonic stem cells were used for blastocyst injection to generate a mouse line homozygous for the *mbd3*$^{Ex1\text{-}Flox}$ allele. These mice were viable and fertile. The Villin-Cre line has been described previously[18]. For tissue collection, mice were killed by cervical dislocation and the intestines were removed and flushed extensively with cold PBS and frozen in liquid nitrogen. For quantitative real-time PCR (qRT–PCR) analysis, total mRNA was isolated from dissected intestines, or from villus and crypt fractions obtained as described before[19]. Results were normalized to those obtained with β-actin and results are presented as fold induction over control mice.

AOM/DSS model of colon carcinoma. The AOM/DSS model used has been described previously[27]. Mice were injected intraperitoneally (i.p.) with 10 mg kg^{-1} body weight of AOM (Sigma) dissolved in physiological saline. Seven days later, 2% DSS was given in the drinking water over 7 days, followed by normal water until the end of the experiment. Body weight was measured every week and the animals were killed 13 weeks after AOM injection for histological analysis. The number of tumours, incidence of tumours and tumour area were determined. For biochemical characterization dissected tumours were snap-frozen in liquid nitrogen and used for qRT–PCR analysis.

DSS model of colon inflammation. The DSS model used has been described previously[28]. Mice were administered orally with 2% DSS in drinking water starting on day 1 and continued until day 6. On day 7, the water was changed to normal drinking water. Body weight was measured every day, and the animals were killed at day 10 for histological analysis.

Immunohistochemical staining. Mice were injected i.p. with 100 mg kg^{-1} BrdU (Sigma) 1.5 h before killing. Mice were euthanized by cervical dislocation, the small intestines dissected out into ice-cold PBS and the faecal contents flushed out with ice-cold PBS. The intestines were cut longitudinally into pieces of similar size, opened out and fixed overnight in 10% neutral buffered formalin, briefly washed with PBS and transferred into 70% ethanol, rolled, processed and embedded into paraffin. Sections were cut at 4 μm for haematoxylin and eosin staining. For immunohistochemistry, antibodies against BrdU (BD Biosciences) were used. To quantify the BrdU-positive cells per crypt, 100 full crypts were scored. For AB/PAS staining, immunohistochemistry and immunofluorescence antibodies against chromogranin-A (Abcam) and β-galactosidase (Acris Antibodies) were used. Anti-lysozyme (DAKO) was used for immunofluorescence as described before[4]. To quantify the AB/PAS^{+} or chromogranin^{+} cells per villus, 100 full villi were scored.

Statistics. Statistical evaluation was performed using the Student's unpaired *t*-test. Data are presented as mean ± s.e.m. and $P \leq 0.05$ was considered statistically significant.